ANOMALY IMAGING FOR STRUCTURAL HEALTH MONITORING EXPLOITING CLUSTERED SPARSITY

Geethu Joseph[†]*, Ahmad B. Zoubi*[*]*, Chandra R. Murthy*[†]*, V. John Mathews*[*]

[†]Dept. of ECE, Indian Institute of Science, Bangalore, India
[*]School of Electrical Engineering and Computer Science, Oregon State University, OR, USA
emails: [†]{geethu, cmurthy}@iisc.ac.in, [*]{zoubia, mathews}@oregonstate.edu.

ABSTRACT

This paper presents a new tomography-based anomaly mapping algorithm for composite structures. The system consists of an array of piezoelectric transducers which sequentially excites the structure and collects the resulting waveform at the remaining transducers. Anomaly indices computed from the sensor waveforms are fed as input to the mapping algorithm. The output of the algorithm is a color map indicating the outline of damage on the structure when present. Unlike prior work on this topic, the algorithm of this paper explicitly accounts for both sparsity and cluster pattern structures that are typical of structural anomalies. Hence, the algorithm of this paper provides excellent reconstruction accuracy by incorporating the available prior information on the anomaly map. Experimental results on a unidirectional composite plate confirms that the algorithm of this paper outperforms two competing methods in terms of reconstruction accuracy.

***Index Terms*—Structural health monitoring, Bayesian learning, structured sparsity.**

I. INTRODUCTION

Many critical infrastructures like aircraft, load bearing walls and oil pipelines use fiber reinforced laminate composite materials. Although composite materials are lightweight, strong, and possess excellent fatigue and corrosion resistance, many inter-laminar defects may show no visible evidence [1], [2]. To ensure the integrity of the structure for safe and efficient operation, it is desirable to embed an inspection system within the structure [3]. An active structural health monitoring (SHM) system consists of an array of transducers that can excite and sense wave propagation within the thickness of the structure. The system periodically excites the structure using the transducers sequentially. The resulting waveforms are collected at the remaining transducers which act as sensors. The collected signal is compared to a set of baseline measurements acquired from the structure prior to deployment. The differences between the two signals are characterized using an anomaly metric. The anomaly metric for all actuator-sensor pairs are used to detect and characterize structural damage.

Several algorithms for anomaly mapping have been presented in the literature. Malyarenko and Hinders [4] described a tomography-based approach to image flaws and corrosion on metallic structures. This approach employs the time difference of arrival of the wave between an actuator and a sensor as the measure of the average properties of the actuator-sensor path. A similar approach is studied for composite plates in [5]. Later, Prasad *et al.* [6] successfully located holes on crossply and quasi-isotropic plates using an iterative algebraic reconstruction technique (ART). The algorithm uses the root-mean-square value between the sensor signals and the corresponding baseline signals as the basis for the reconstruction algorithm. Gao *et al.* [7] proposed the reconstruction algorithm for probabilistic inspection of damage (RAPID) for damage mapping. Although low in complexity, the algorithm design does not consider any particular signal structure associated with the anomaly map. Recently, Zoubi and Mathews [8], [9] developed an anomaly mapping algorithm that uses the sparse nature of damage distribution on structures. However, the sparsity model in the anomaly map is significantly more structured and exhibits a two-dimensional clustered pattern. Therefore, we present a new solution exploiting the two-dimensional clustered sparsity pattern as a prior information to the anomaly map reconstruction problem.

This paper presents a new algorithm for anomaly imaging, based on ART and the two-dimensional pattern coupled sparse Bayesian learning algorithm. The algorithm takes a set of Lamb wave measurements collected on the structure as input, and outputs an anomaly map from which one can estimate the boundaries of damage on the structure. To the best of our knowledge, this paper is the first to exploit the two-dimensional clustered sparsity pattern of the anomaly map to improve damage mapping accuracy. Experimental results on a unidirectional composite plate show that the

The work of G. Joseph was supported in part by an Intel India PhD fellowship. This work was supported in part by a research grant from the Ministry of Electronics and Information Technology, Govt. of India.

method of this paper provides more accurate estimates of the damage boundaries than two competing algorithms.

II. SYSTEM MODEL

We consider an SHM system that uses a set of m transducers where each transducer can act as a wave sensor or a wave actuator, as needed. The structure is excited sequentially by the transducers to obtain an anomaly metric (index) for each signal path connecting the actuator-sensor pairs. The goal is to estimate the anomaly map of the structure, using the $K = m(m-1)$ damage indices thus obtained.

To reconstruct the anomaly map, we employ a grid architecture where the spatially continuous map is discretized into N cells or pixels using a grid as shown in Figure 1. The damage value associated with each pixel indicates the state of the corresponding part of the structure. Thus, our goal reduces to computing the map value at each pixel using the measured anomaly indices. The mathematical model relating anomaly map values and the damage indices is adopted from the ART framework. Here, the damage indices are assumed to be a linear combination of the pixel values weighted with the length of the direct path between the actuator-sensor pair that crosses the pixel [10]. For instance, in Figure 1, the damage index for the signal path between the sensor-actuator pair depends on the pixels which are marked in blue. This linear relationship can be written as

$$\boldsymbol{y} = \boldsymbol{L}\boldsymbol{x}, \tag{1}$$

where $\boldsymbol{y} \in \mathbb{R}^K$ is obtained by stacking the damage metrics into a column vector. The column vector $\boldsymbol{x} \in \mathbb{R}^N$ is the vector of the pixel values or the vectorized version of the discretized anomaly map. The $(i,j)^{\text{th}}$ entry of the matrix $\boldsymbol{L} \in \mathbb{R}^{K\times N}$ is the length of i^{th} line segment that overlaps pixel j, as illustrated using Figure 1. Hence, the map recovery problem is equivalent to the recovery of $\boldsymbol{x}$ from (1) when $\boldsymbol{y}$ and $\boldsymbol{L}$ are known. In the next section, we present the algorithm to recover the discretized anomaly map which utilizes the sparse and clustered structures associated with the unknown map.

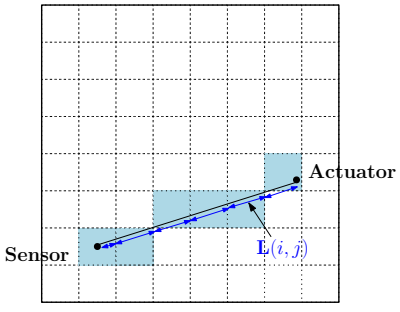

Fig. 1: The figure shows i^{th} sensor-actuator pair and the direct path between them. The pixels in blue correspond to the nonzero entries of j^{th} row of $\boldsymbol{L}$, and the non-zero value equals the length of the path overlapping the pixel.

III. MAP RECOVERY ALGORITHM

We recover the unknown $\boldsymbol{x}$ by exploiting two underlying structures in the signal:

1) Anomaly areas on the structure are usually small compared to its overall size, which makes $\boldsymbol{x}$ naturally sparse.
2) The anomaly areas occupy a small continuous region of the structure. Therefore, the anomaly map exhibits two-dimensional cluster patterns, also known as block-sparsity.

Several recovery algorithms that exploit block-sparsity have been proposed in the literature. Examples include block-OMP [11], mixed ℓ_2/ℓ_1 norm-minimization [12], group LASSO [13] and block-sparse Bayesian learning [14]. These algorithms require *apriori* knowledge of the block boundaries. However, in our case, the two-dimensional cluster pattern is not known as it depends on the unknown location and shape of the anomaly area. Recently, a new approach has been proposed to tackle the difficulty of unknown block boundaries using the sparse Bayesian learning (SBL) framework [15], [16]. Moreover, the SBL-based algorithms are known to have superior performance compared to convex relaxation or greedy approaches. Hence, we use the *pattern-coupled (PC) SBL* algorithm to exploit the two-dimensional block-sparse structure.

In the SBL framework, we use a fictitious prior on the unknown signal which promotes the underlying signal structures. To account for the two-dimensional block-sparse structure, a pattern-coupled Gaussian hierarchical prior is imposed on $\boldsymbol{x}$. The use of hyper-parameters associated with each entry of $\boldsymbol{x}$ in the hierarchical Gaussian prior is known to promote sparsity. In addition, two-dimensional block-sparse structure is captured by imposing dependency between the hyper-parameters associated with each entry and that of its neighboring entries: $\boldsymbol{x} \sim \mathcal{N}(\boldsymbol{x}; \boldsymbol{0}, \boldsymbol{\Gamma})$, where $\boldsymbol{\Gamma} \in \mathbb{R}^{N\times N}$ is a diagonal matrix with diagonal entries:

$$\gamma_i^{-1} = \boldsymbol{\alpha}_i + \beta \sum_{j\in\mathcal{B}(i)} \boldsymbol{\alpha}_j, \tag{2}$$

Here, $\boldsymbol{\alpha} \in \mathbb{R}^N$ is a vector of non-negative hyperparameters, $\beta \in [0,1]$ is the coupling parameter, and $\mathcal{B}(i)$ is the set of neighboring entries of $\boldsymbol{x}_i$ in the two-dimensional signal. Due to the interdependence on the priors, the entry $\boldsymbol{x}_i$ is driven to zero if α_i or any of its neighboring hyperparameters goes to infinity. The shared hyperparameters enables the prior to flexibly model any block-sparse structure, without pre-specifying the block boundaries.

Using the model in (2), as in conventional SBL, we use type II maximum likelihood estimation for $\boldsymbol{x}$. In other words, we first estimate the hyperparamters of the imposed prior which in turn yields an estimate of the sparse $\boldsymbol{x}$. The hyperparameters are obtained using the expectation-maximization (EM) algorithm, where the sparse vectors are treated as hidden variables. We summarize the pseudo-code for anomaly mapping in Algorithm 1. For detailed derivation of the PC-SBL algorithm, please refer to [15], [16].

Algorithm 1 The PC-SBL Recovery Algorithm

Input: $\boldsymbol{y}$ and $\boldsymbol{L}$
  Parameters: Coupling coefficient β, Tolerance ϵ
  Initialize: $\boldsymbol{\alpha}^{(0)}$, $\sigma^{2(0)}$, $c = d = 10^{-4}$
  while $\left\|\boldsymbol{\alpha}^{(r)} - \boldsymbol{\alpha}^{(r-1)}\right\| \leq \epsilon$ **and** $\left|\sigma^{2(r)} - \sigma^{2(r-1)}\right| \leq \epsilon$ **do**
    for $r = 1, 2, \ldots$ **do**
      $\boldsymbol{\gamma}_i = \left(\boldsymbol{\alpha}_i^{(r-1)} + \beta \sum_{j \in \mathcal{B}(i)} \boldsymbol{\alpha}_j^{(r-1)}\right)^{-1}$, $i = 1,2,\ldots,N$
      $\boldsymbol{\Sigma} = \left(\sigma^{-2(r-1)} \boldsymbol{L}\boldsymbol{L}^{\mathrm{T}} + \mathrm{Diag}\left\{\boldsymbol{\gamma}\right\}\right)^{-1}$
      $\boldsymbol{\mu} = \sigma^{-2(r-1)} \boldsymbol{\Sigma} \boldsymbol{L}^{\mathrm{T}} \boldsymbol{y}$
      $\sigma^{2(r)} = K + 2c \left(2d + \left\|\boldsymbol{y} - \boldsymbol{L}\boldsymbol{\mu}\right\|^2 + \mathrm{Tr}(\boldsymbol{L}\boldsymbol{L}^T \boldsymbol{\Sigma})\right)^{-1}$
      for $i = 1, 2, \ldots, N$ **do**
        $\boldsymbol{\alpha}_i^{(r)} = 2 \left(\boldsymbol{\mu}_i^2 + \boldsymbol{\Sigma}_{ii} + \beta \sum_{j \in \mathcal{B}(i)} \boldsymbol{\mu}_j^2 + \boldsymbol{\Sigma}_{jj}\right)^{-1}$
      end for
    end for
  end while
Output: $\boldsymbol{x} = \boldsymbol{\mu}$

Although (1) does not assume any model mismatch, PC-SBL can handle noisy measurements. The PC-SBL based reconstruction can also be applied to other ART-based tomographic imaging methods such as MRI, for cancer detection.

IV. EXPERIMENTAL RESULTS

The experiments described here were conducted on a $41''$ wide, $40''$ long and $0.1''$ thick, unidirectional composite panel made out of 8 IM7/8552 carbon fiber plies. Thirty two piezoelectric transducers were attached to the plate covering the middle $33'' \times 32''$ region of the plate. The excitation signal used was a linear chirp with bandwidth [150,300 kHz] and the resulting waveforms were acquired with a 2×10^6 samples/second sampling rate. First, the baseline signals were collected before impact damage was introduced into the structure. Then, we impacted the structure on different locations to create damage, and the test signals were acquired after each impact experiment. Other computational details are as follows:

Choice of damage index: We first applied a mode decomposition algorithm based on cross Wigner-Ville-distribution of the received signal. The anomaly indices were computed using the extracted first arriving mode of the measured signal and the baseline signal, as proposed in [8], [9], [17].

Multi-grid architecture: The virtual grid on the structure is assumed to be rectangular with 22×22 pixels. Since the choice of the grid structure is arbitrary, we used the multi-grid architecture to improve the reconstruction accuracy. We reconstructed the map using 20 different grids on the structure, then, interpolated them to obtain a map on a high-resolution grid. The interpolated grids were 200×200 pixels. The final estimate of the anomaly map was obtained by averaging over these 20 maps. Further details on the multi-grid averaging approach can be found in [18].

Algorithm tuning: From our experiments, we have seen that the choice of parameters β and ϵ of Algorithm 1 is not critical. For the results presented here, we choose $\beta = 1$ and $\epsilon = 10^{-6}$. Also, in the algorithm, we adopt a pruning operation for faster convergence. At each iteration, we pruned those small coefficients associated with hyperparameters $\boldsymbol{\alpha}_i$ greater than 10^{11} times the minimum value.

Estimation of anomaly boundaries: The damage area was estimated as the locations on the structure where the estimated map value was greater than some threshold, and the threshold is calculated using training data.

Recovery accuracy metric: We used the Sørenson-Dice index (also known as F1 score), which computes the correlation between two data sets A and B as $\frac{2|A \cap B|}{|A| + |B|}$. Here, the anomaly map obtained using an A-scan device (manual non-destructive evaluation technique) was used as the ground truth.

To illustrate the performance of our algorithm, we compare the algorithm of this paper based on PC-SBL with two state-of-the-art algorithms: a least-squares (LS) based damage mapping algorithm [18] and a LASSO based damage mapping algorithm [8], [9]. Figure 2 shows the reconstructed map of the composite plate obtained using three algorithms after impact experiments. Each row corresponds to an experiment, and each column corresponds to an algorithm. The blue outlines in the maps represent the boundaries of the anomaly estimated using A-scan. The extent of the anomaly estimated by each algorithm is shown in red. We also provide the Sørenson-Dice similarity index of the estimated boundaries in the caption of each figure.

From Figure 2, we see that, compared to the LS-based method (first column), the algorithm of this paper (last column) has fewer false alarms. Also, compared to the LASSO based method (middle column), the algorithm of this paper gives better estimate of the damage boundaries, which is evident from the Sørenson-Dice index. Overall, the results clearly indicate that the map reconstructed by the PC-SBL algorithm identifies the true anomalies in the structure more closely compared to the other approaches.

V. CONCLUSION

This paper presented a new algorithm for anomaly map reconstruction for health monitoring of composite structures. We utilized the two-dimensional clustered sparse structure associated with structural damage to present a new map reconstruction algorithm. Using a data set obtained from impact experiments, we demonstrated the superiority of our algorithm compared to two competing algorithms available in the literature. The results showed that exploiting any underlying structure of the damage improves the map reconstruction accuracy. However, we did not exploit the non-negative nature of the anomaly map. Modifying the PC-SBL prior to account for non-negativity is an interesting avenue for future work.

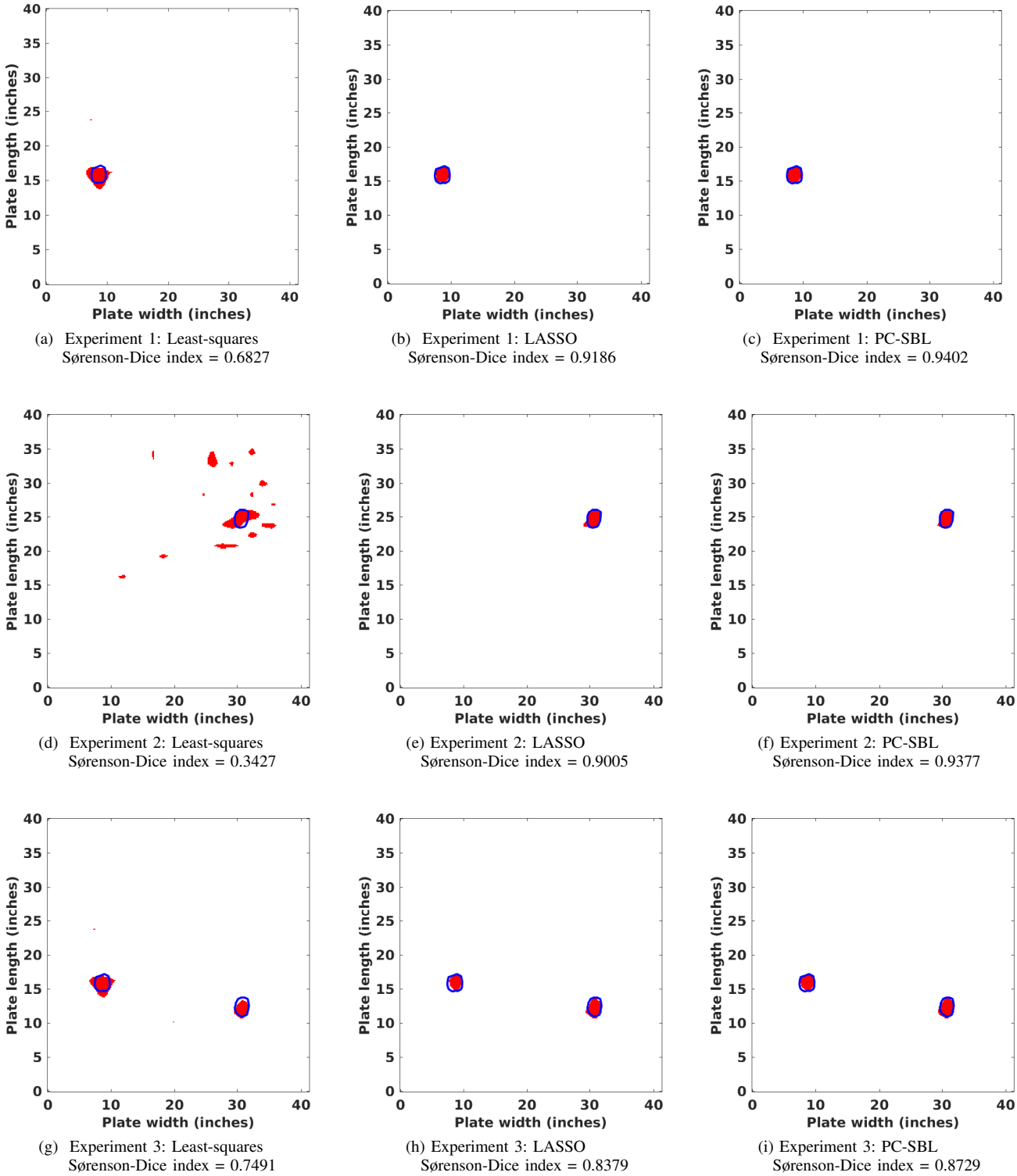

(a) Experiment 1: Least-squares
Sørenson-Dice index = 0.6827

(b) Experiment 1: LASSO
Sørenson-Dice index = 0.9186

(c) Experiment 1: PC-SBL
Sørenson-Dice index = 0.9402

(d) Experiment 2: Least-squares
Sørenson-Dice index = 0.3427

(e) Experiment 2: LASSO
Sørenson-Dice index = 0.9005

(f) Experiment 2: PC-SBL
Sørenson-Dice index = 0.9377

(g) Experiment 3: Least-squares
Sørenson-Dice index = 0.7491

(h) Experiment 3: LASSO
Sørenson-Dice index = 0.8379

(i) Experiment 3: PC-SBL
Sørenson-Dice index = 0.8729

Fig. 2: Comparison of the damage outlines estimated by three different algorithms along with corresponding Sørenson-Dice similary index. The method of this paper provides the best results out of the three methods.

VI. REFERENCES

[1] B. W. Drinkwater and P. D. Wilcox, "Ultrasonic arrays for non-destructive evaluation: A review," *NDT & E International*, vol. 39, no. 7, pp. 525–541, Oct. 2006.

[2] R. Geng, "Modern acoustic emission technique and its application in aviation industry," *Ultrasonics*, vol. 44, pp. e1025–e1029, Dec. 2006.

[3] K. Worden, C. R. Farrar, G. Manson, and G. Park, "The fundamental axioms of structural health monitoring," in *Proc. Math. Phys. Eng. Sci.*, Jun. 2007.

[4] E. V. Malyarenko and M. K. Hinders, "Fan beam and double crosshole Lamb wave tomography for mapping flaws in aging aircraft structures," *J. Acoust. Soc. Am*, vol. 108, no. 4, pp. 1631–1639, Oct. 2000.

[5] K. R. Leonard, E. V. Malyarenko, and M. K. Hinders, "Ultrasonic Lamb wave tomography," *Inverse Probl.*, vol. 18, no. 6, pp. 1795–1808, Nov. 2002.

[6] S. M. Prasad, K. Balasubramaniam, and C. Krishnamurthy, "Structural health monitoring of composite structures using Lamb wave tomography," *Smart Mater. Struct.*, vol. 13, no. 5, pp. N73–N79, Jul. 2004.

[7] H. Gao, Y. Shi, J. Rose, D. O. Thompson, and D. E. Chimenti, "Guided wave tomography on an aircraft wing with leave in place sensors," in *Proc. AIP*, Apr. 2005.

[8] A. B. Zoubi and V. J. Mathews, "Anomaly imaging using decomposed Lamb wave modes," in *Proc. IWSHM*, Sep. 2017.

[9] A. B. Zoubi, S. Kim, D. O. Adams, and V. J. Mathews, "Lamb wave mode decomposition based on cross-Wigner-Ville distribution and its application to anomaly imaging for structural health monitoring," *IEEE Trans. Ultrason., Ferroelectr., Freq. Control*, 2018, (Accepted).

[10] D. Wang, W. Zhang, X. Wang, and B. Sun, "Lamb-wave-based tomographic imaging techniques for hole-edge corrosion monitoring in plate structures," *Materials*, vol. 9, no. 11, p. 916, Nov. 2016.

[11] Y. C. Eldar, P. Kuppinger, and H. Bolcskei, "Block-sparse signals: Uncertainty relations and efficient recovery," *IEEE Trans. Signal Process.*, vol. 58, no. 6, pp. 3042–3054, Jun. 2010.

[12] Y. C. Eldar and M. Mishali, "Robust recovery of signals from a structured union of subspaces," *IEEE Trans. Inf. Theory*, vol. 55, no. 11, pp. 5302–5316, Nov. 2009.

[13] M. Yuan and Y. Lin, "Model selection and estimation in regression with grouped variables," *J. Royal Stat. Soc.*, vol. 68, no. 1, pp. 49–67, Feb. 2006.

[14] Z. Zhang and B. D. Rao, "Sparse signal recovery with temporally correlated source vectors using sparse bayesian learning," *IEEE J. Sel. Topics Signal Process.*, vol. 5, no. 5, pp. 912–926, Sep. 2011.

[15] J. Fang, Y. Shen, H. Li, and P. Wang, "Pattern-coupled sparse Bayesian learning for recovery of block-sparse signals," *IEEE Trans. Signal Process.*, vol. 63, no. 2, pp. 360–372, Jan. 2015.

[16] J. Fang, L. Zhang, and H. Li, "Two-dimensional pattern-coupled sparse Bayesian learning via generalized approximate message passing," *IEEE Trans. Image Process.*, vol. 25, no. 6, pp. 2920–2930, Jun. 2016.

[17] A. B. Zoubi, V. J. Mathews, J. Harley, and D. Adams, "Lamb waves mode decomposition using the cross-Wigner-Ville distribution," in *Proc. IWSHM*, Sep. 2015.

[18] V. J. Mathews, "Damage mapping in structural health monitoring using a multi-grid architecture," in *Proc. AIP*, vol. 1650, no. 1, Mar. 2015, pp. 1247–1255.